Closed-Loop Control of ^{3}He Nuclear Spin Oscillator: Implementation via Metastability Exchange Optical Pumping

Liangyong Wu[1], Changbo Fu[1*], and Haiyang Yan[2*]

[1]*Key Laboratory of Nuclear Physics and Ion-beam Application (MOE), Institute of Modern Physics, Fudan University, Shanghai 200433, China*
[2]*Institute of Fundamental Physics and Quantum Technology, and School of Physical Science and Technology, Ningbo University, Ningbo 315211, China*

(Received 7 July 2025; accepted manuscript online 13 October 2025)

Achieving long spin coherence times is crucial for quantum precision measurements, and closed-loop control techniques are often employed to accomplish this goal. Here, we demonstrate the impact of closed-loop feedback control on nuclear spin precession in a metastability exchange optical pumping (MEOP)-based polarized ^{3}He system. We analyze the effects of feedback theoretically and validate our predictions experimentally. With optimized feedback parameters, the spin coherence time T_2 is extended by an order of magnitude. When the feedback strength surpasses a critical threshold, robust maser oscillations are spontaneously excited, demonstrating remarkable resistance to environmental noise and maintaining stable oscillation. This proof-of-principle experiment highlights the viability of MEOP-based ^{3}He spin oscillators, especially in low-frequency domains. The operational simplicity and easy integration associated with MEOP-based systems make them particularly promising for fast, high-precision magnetic field measurements.

DOI: 10.1088/0256-307X/42/12/120301 CSTR: 32039.14.0256-307X.42.12.120301

1. Introduction. The precision measurement of Zeeman splitting plays a central role in a wide range of applications, including magnetic field sensing in diverse environments,[1,2] g-factor determination,[3,4] inertial navigation using nuclear magnetic resonance gyroscopes,[5,6] and searches for electric dipole moments,[7,8] as well as exotic spin-dependent interactions beyond the Standard Model.[9–13] To date, spin-based quantum sensors have demonstrated state-of-the-art sensitivity in measuring Zeeman splitting in magnetometry applications.[14] The fundamental operating principle of such sensors is to detect the Larmor precession frequency of polarized spins subjected to the magnetic field of interest. The spin precession can be monitored either in free-induction decay mode or in a sustained oscillatory regime, corresponding to atomic magnetometers and spin masers, respectively. The sensitivity of spin-based sensors to magnetic fields is primarily determined by two key factors: the signal-to-noise ratio (SNR) and the spin coherence time.[1] The SNR can be enhanced through methods such as Fermi-contact interaction with alkali atoms[15] or the use of multipass vapor cells.[16,17] As for coherence time, various strategies have been proposed to extend it in atomic magnetometers, including the use of anti-relaxation coatings,[18,19] the spin-exchange-relaxation-free regime,[20,21] and compensation of magnetic field gradients.[22,23] However, these approaches often require carefully engineered conditions, such as high-quality atomic vapor cells and effective magnetic shielding.

While in a spin maser, spin precession can be sustained indefinitely, ensuring that both coherence and SNR remain stable throughout the measurement. This characteristic makes the maser an attractive platform for high-precision frequency measurements. Maser oscillation can, in principle, be sustained in any spin system, provided that appropriate feedback is applied. Even in the free precession decay regime, feedback can be employed to prolong coherence time and improve sensitivity.[24,25] The central concept of the spin maser is to employ feedback to sustain spin precession continuously. This feedback loop effectively closes the system, converting it into a closed-loop spin oscillator. The idea of using feedback to maintain oscillatory behavior is well-established, with parallels found in optical lasers[26] and atomic clocks.[27]

In nuclear spin masers, the feedback signal originates directly from the spin precession, typically detected by either pickup coils or optical methods. Pickup coil detection, based on electromagnetic induction, is effective at high frequencies but demands careful coil tuning to match resonance frequencies and often requires operation in high-density noble gases or at elevated frequencies to achieve sufficient feedback strength.[28–31] In contrast, optical detection via the Faraday rotation effect offers superior sensitivity and facilitates efficient maser operation even at ultra-low frequencies. Traditionally, optical detection of nuclear spin masers has employed spin-exchange optical pumping (SEOP), where spin-exchange interactions between alkali and noble gases read out nuclear

*Corresponding authors. Email: cbfu@fudan.edu.cn; yanhaiyang@nbu.edu.cn
© 2025 Chinese Physical Society and IOP Publishing Ltd. All rights, including for text and data mining, AI training, and similar technologies, are reserved.

spin precession and feed back to the driving radio frequency (RF) coils.[32–35] While SEOP-based nuclear spin masers, particularly the Rb–Xe system, have been extensively studied,[36–41] relatively less attention has been devoted to the ^{3}He system.[42] However, compared to xenon, ^{3}He exhibits a larger gyromagnetic ratio and a smaller atomic radius, which inherently enhances its sensitivity to weak magnetic fields and enables longer spin coherence times. Thus, we explore the potential of closed-loop maser oscillation in metastability exchange optical pumping (MEOP)-polarized ^{3}He. Unlike SEOP, MEOP operates without heating, significantly reducing temperature-induced instabilities, and achieves saturated nuclear polarization within roughly one minute, considerably faster than SEOP. Such characteristics make MEOP-polarized ^{3}He highly attractive for applications requiring rapid deployment and long-term stability. For instance, stable precession of MEOP-polarized ^{3}He has already been utilized to detect subtle frequency shifts induced by exotic spin-dependent interactions beyond the Standard Model,[12,23] and MEOP-based absolute magnetometers have demonstrated ppb-level precision in strong-field magnetic measurements, potentially setting a new standard in absolute magnetometry.[2] Furthermore, MEOP typically operates under low-pressure conditions (∼torr), where motional narrowing effectively suppresses magnetic-field-gradient-induced frequency shifts and decoherence,[43] further enhancing maser performance. Given these advantages, the MEOP-based ^{3}He spin maser emerges as a highly promising platform for long-term, high-precision measurements.

In this work, we investigate the feedback effect on the precession of ^{3}He nuclear spins polarized by the MEOP technique. The spin dynamics are modeled using the Bloch equations and analyzed across two distinct regimes of feedback strength G_f: the spin decay region and the spin maser region. In the spin decay region, feedback may either extend or reduce the coherence time, depending on its strength and phase. Upon entering the spin maser region, the system exhibits self-sustained spin oscillations that are robust against perturbations.

2. Feedback-Driven Bloch Equations. The dynamics of polarized ^{3}He nuclear spins, subjected to a magnetic field $\boldsymbol{B}(t) = B_\mathrm{f}(t)\hat{y} + B_0\hat{z}$ where B_0 is the static field along the z-axis and $B_\mathrm{f}(t)$ is the feedback-driven field applied along the y-axis, are governed by the Bloch equations,[44]

$$\begin{aligned}\frac{\mathrm{d}}{\mathrm{d}t}\boldsymbol{M}(t) &= \gamma\boldsymbol{M}(t)\times\boldsymbol{B}(t) - \Gamma_2\boldsymbol{M}_\perp(t)\\ &\quad + R_\mathrm{op}[M_0 - M_z(t)]\hat{z},\end{aligned} \tag{1}$$

where $\boldsymbol{M}(t)$ is the spin magnetization, decomposed into components parallel and perpendicular to $\hat{z}$ as $M_z\hat{z}$ and $\boldsymbol{M}_\perp$, respectively; $\gamma = 2\pi\times 3.24\,\mathrm{kHz/G}$ is the gyromagnetic ratio of the ^{3}He nucleus; Γ_2 denotes the transverse relaxation rate; R_op is the optical pumping rate; and M_0 is the equilibrium magnetization.

In the feedback control scheme illustrated in Fig. 1, the precession of the transverse magnetization generates the RF feedback field, which is subsequently amplified

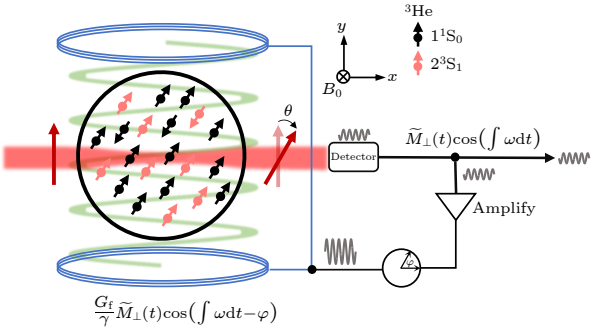

Fig. 1. Diagram of closed-loop control on ^{3}He spin precession.

and applied along the $\hat{y}$ direction, rather than being driven by an external excitation source. For convenience, the transverse magnetization is represented as a phasor,[5]

$$M_+(t) = M_x + \mathrm{i}M_y = \widetilde{M}_\perp(t)\mathrm{e}^{-\mathrm{i}\int\omega\mathrm{d}t}, \tag{2}$$

where ω is the precession frequency about the z-axis. Since the feedback signal is derived from the x-component of the magnetization, $\hat{x}\cdot\boldsymbol{M}_\perp(t)$, and a phase shift is introduced by the feedback loop, the feedback magnetic field can be written as[38,45]

$$B_\mathrm{f}(t) = \frac{G_\mathrm{f}}{\gamma}\widetilde{M}_\perp(t)\cos\Big(\int\omega\mathrm{d}t - \varphi\Big), \tag{3}$$

where G_f is a coefficient proportional to, and tunable by, the feedback gain, incorporating factors such as magnetization strength, coil configuration, and distance—ultimately determining the amplitude of the RF feedback field—and φ is the phase factor.

Applying Eq. (3), the feedback-driven Bloch Eq. (1) is reduced to

$$\begin{aligned}\frac{\mathrm{d}}{\mathrm{d}t}\widetilde{M}_\perp &= \mathrm{i}(\omega-\gamma B_0)\widetilde{M}_\perp - \Big(\Gamma_2 + \frac{1}{2}G_\mathrm{f}M_z\mathrm{e}^{\mathrm{i}\varphi}\Big)\widetilde{M}_\perp\\ &\quad - \frac{1}{2}G_\mathrm{f}M_z\mathrm{e}^{\mathrm{i}(\int 2\omega\mathrm{d}t-\varphi)}\widetilde{M}_\perp,\\ \frac{\mathrm{d}}{\mathrm{d}t}M_z &= \frac{1}{2}G_\mathrm{f}\widetilde{M}_\perp^2\cos\varphi + R_\mathrm{op}(M_0 - M_z)\\ &\quad + \frac{1}{2}G_\mathrm{f}\widetilde{M}_\perp^2\cos\Big(\int 2\omega\mathrm{d}t - \varphi\Big).\end{aligned} \tag{4}$$

Under the rotating-wave approximation (RWA), the rapidly oscillating terms associated with 2ω are averaged out. As a result, the instantaneous resonance frequency $\omega(t)$ and the transverse relaxation rate $\Gamma(t)$ can be extracted from the imaginary and real parts, respectively, of the first equation in Eq. (4),

$$\begin{aligned}\omega(t) &= \gamma B_0 + G_\mathrm{f}M_z(t)\sin\varphi/2,\\ \Gamma(t) &= \Gamma_2 + G_\mathrm{f}M_z(t)\cos\varphi/2.\end{aligned} \tag{5}$$

Assuming a steady-state oscillation, we set the time derivatives in Eq. (4) to zero, yielding:

$$\begin{aligned}&\text{Decay mode}: \begin{cases} M_z^\mathrm{eq} = M_0,\\ \widetilde{M}_\perp^\mathrm{eq} = 0,\end{cases}\\ &\text{Maser mode}: \begin{cases} M_z^\mathrm{eq} = -\frac{2\Gamma_2}{G_\mathrm{f}\cos\varphi},\\ \widetilde{M}_\perp^\mathrm{eq} = \sqrt{-\frac{2R_\mathrm{op}}{G_\mathrm{f}\cos\varphi}\Big[M_0 + \frac{2\Gamma_2}{G_\mathrm{f}\cos\varphi}\Big]}.\end{cases}\end{aligned} \tag{6}$$

In the decay mode, when the transverse component is sufficiently small such that $|M_\perp| \ll M_z$, the longitudinal magnetization M_z can be approximated by its equilibrium value M_0. As a result, the transverse magnetization evolves according to a free induction decay (FID) pattern with a modified decay rate, given by

$$\Gamma = \Gamma_2 + G_\mathrm{f} \cos\varphi \frac{M_0}{2}. \tag{7}$$

Accordingly, the decay mode can be divided into two regions: a coherence-time-enhanced (CTE) region, where $\cos\varphi < 0$, and a coherence-time-reduced (CTR) region, where $\cos\varphi > 0$, noting that G_f is positive. The enhanced coherence time has been exploited in Refs. [24,25] to improve magnetometric sensitivity. Tang *et al.*[24] employed feedback to narrow the magnetic resonance linewidth of ^{133}Cs, achieving a 22-fold improvement in measurement sensitivity. In the work of Xu *et al.*,[25] feedback was used to extend the coherence time of polarized ^{129}Xe, thereby enhancing the sensitivity of a spin amplifier based on a ^{87}Rb–^{129}Xe comagnetometer. In contrast, the reduced coherence time in the corresponding feedback regime improves the system's ability to respond to rapid changes and broadens its operational bandwidth.

In the maser mode, since the magnitude of the magnetization must be positive, the phase condition $\pi/2 < \varphi < 3\pi/2$ and the strength condition $-G_\mathrm{f}\cos\varphi M_0 > 2\Gamma_2$ must be satisfied. The steady-state amplitude of the transverse magnetization reaches its maximum when the feedback coefficient satisfies $G_\mathrm{f}\cos\varphi = -4\Gamma_2/M_0$, which is exactly twice the threshold value required to excite the maser oscillation. In this case, the accuracy of determining the frequency from the maser is optimal due to the best SNR.[23] The frequency shift indicated by Eq. (5) is one of the systematic errors that influence the stability of the maser due to fluctuations in the feedback loop. This shift degrades the maser's performance over the long term. Substituting the steady-state value of M_z into Eq. (5), one obtains the frequency offset of the maser at equilibrium: $\Delta\omega = -\Gamma_2 \tan\varphi$. It is noted that the frequency shift depends solely on the phase of the feedback and vanishes when $\varphi = \pi$, i.e., when the feedback is exactly out of phase with the magnetization precession along the x-axis. On the other hand, the shift is also proportional to the spin's transverse relaxation rate, indicating that spin species with longer relaxation times should exhibit better frequency stability when used in masers. For hyperpolarized noble gases, ^{3}He exhibits the longest coherence time, up to tens of hours, making it the most suitable choice for a spin maser in theory. In experiments, the relaxation time is usually limited by magnetic field gradients and can be extended by reducing the field strength.[43] Therefore, masers operating at low frequencies (∼Hz) are inherently less sensitive to frequency shifts caused by phase noise. Moreover, a longer coherence time reduces the feedback strength required to sustain maser oscillation.

3. Experimental Setup. The experimental setup is schematically shown in Fig. 2. A cylindrical cell ($\phi = 5$ cm, $L = 5$ cm) filled with ^{3}He gas at a pressure of 100 Pa is

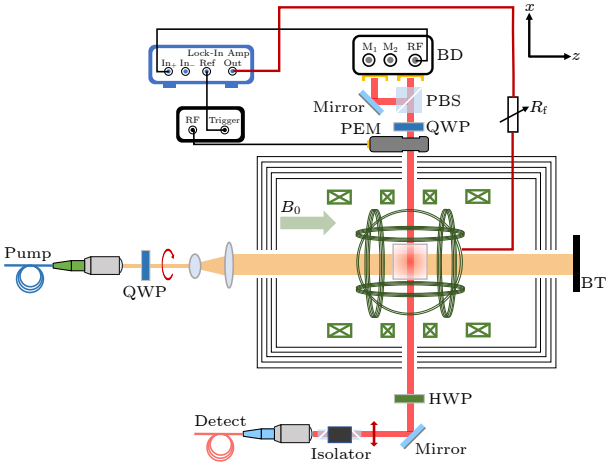

Fig. 2. Experimental setup and basic concept of the feedback-driven ^{3}He nuclear oscillator based on MEOP. The precession of the polarized ^{3}He is detected using optical and lock-in amplification methods. The demodulated and amplified signal is then fed back to the driving coils—a pair of Helmholtz coils aligned along the y-axis—where a variable resistor R_f in the loop adjusts the feedback current, and consequently, the strength of the driving field. PBS: Polarizing Beam Splitter; QWP: Quarter-Wave Plate; HWP: Half-Wave Plate; BT: Beam Trap; BD: Balanced Detector; PEM: Photoelastic Modulator.

placed at the center of a uniform magnetic field. The nuclear spin of ^{3}He is polarized via MEOP,[34] which consists of two key processes: (i) optical pumping of ^{3}He atoms in the metastable state using circularly polarized light on the $2^3\mathrm{S}$–$2^3\mathrm{P}$ transition, and (ii) transfer of nuclear polarization to the ground-state atoms via metastability-exchange collisions (MECs). In the experiment, a weak RF discharge at 1.16 MHz is applied to the cell through two attached copper wires, exciting the ^{3}He atoms and maintaining approximately 10^{-6} of them in the metastable state. Polarization of the metastable atoms along the z-axis is achieved with a circularly polarized pump beam of 0.8 W power at a wavelength of 1083.3538 nm, corresponding to the C_8 transition between the hyperfine levels $|2^3\mathrm{S}_1,\ F = 1/2\rangle$ and $|2^3\mathrm{P}_0,\ F = 1/2\rangle$. Through MECs, the nuclear polarization established in the metastable state is transferred to the ground state, producing nuclear spin–polarized ^{3}He atoms. Under our experimental conditions, the optical pumping rate is $R_\mathrm{op} \sim 0.0625\,\mathrm{s}^{-1}$, and the saturated polarization, proportional to M_0, reaches approximately 77%. A linearly polarized detection laser (power: ∼1 mW; wavelength: 1083.331 nm) propagating along the x-axis is used to monitor the transverse magnetization component M_x. The polarization rotation of the probe beam is proportional to M_x and is detected using homodyne detection.[46] To improve the SNR, the probe polarization is modulated at 50 kHz using a photoelastic modulator (PEM), and the signal is extracted using a lock-in amplifier. The output of the lock-in amplifier, after appropriate adjustments, is fed back to a pair of Helmholtz coils aligned along the y-axis to generate a uniform feedback magnetic field. A variable resistor R_f in the feedback loop controls the feedback current, and consequently, the strength of the feedback field.

For the setup used in this work, we found that a phase shifter is not required to establish maser oscillation in a low magnetic field. The explanation is as follows. Due to the strong coupling between the metastable and ground states via MECs, the response of the angular momentum in the metastable state, such as the $F = 3/2$ hyperfine level, to excitations in the ground state is given by [47]

$$\langle F_+\rangle_{3/2} = \frac{10}{9}\left(\frac{1}{1-\mathrm{i}\omega_e\tau} + \frac{2}{1-4\mathrm{i}\omega_e\tau}\right)\langle I_+\rangle, \qquad (8)$$

where $I_+ = I_x + \mathrm{i}I_y$ represents the nuclear spin of the ground state, and $F_+ = F_x + \mathrm{i}F_y$ denotes the angular momentum of the metastable state, ω_e ($2\pi \times 2.8\,\mathrm{MHz/G}$) is the Larmor frequency of the electron, and τ ($\sim 10^{-7}\,\mathrm{s}$) is the mean free time for MECs. In this experiment, the applied magnetic field is approximately 0.01 G, resulting in a phase difference of about 0.1 rad between $\langle F_+\rangle$ and $\langle I_+\rangle$. Since the output signal of the balanced detector is proportional to $\langle F_x\rangle$, [46] the relative phase between the feedback signal and M_x is approximately $\varphi \sim 0$. Therefore, by reversing the polarity of the lock-in amplifier's output—achievable via the lock-in's internal function—the phase of the feedback signal can be toggled between 0 and π, thereby satisfying the phase condition required for maser operation.

4. Results and Discussions. We first adjust the feedback strength to investigate its effect on the coherence time T_2 of ^{3}He. The coherence time T_2 at different feedback strengths ($G_f \propto 1/R_f$) is determined by fitting the FID signal of the transverse magnetization excited by an RF pulse. Figure 3(a) shows three types of time-domain FID signals, from top to bottom, corresponding to the CTE, no-feedback, and CTR cases, respectively. The scatter points in Fig. 3(b) show the measured T_2 values for different feedback strengths. At the same time, the dashed line represents the theoretical prediction, Eq. (7), under the RWA approximation. To validate this approximation, results from numerical solutions of the feedback-driven Bloch Eq. (1) are also included and are shown as the solid line in Fig. 3(b). When the feedback is turned off, the coherence time of the ^{3}He spin is observed to be approximately 15 s. By carefully adjusting the variable resistor R_f, we achieve a maximum T_2 of about 130 s at a feedback strength of $1/750\,\Omega^{-1}$. Compared to the case without feedback, the coherence time is enhanced by nearly an order of magnitude, improving the frequency resolution, as determined by the Cramér–Rao lower bound, [48] from 10 μHz to 100 nHz. Under the present conditions, achieving such a significant improvement in coherence time is challenging, as the system becomes unstable when the feedback strength approaches the maser threshold—tiny perturbations can trigger self-oscillation of the spin precession. Reversing the output signal of the lock-in amplifier leads to a suppression of the coherence time. For a feedback strength of $1/50\,\Omega^{-1}$, the coherence time is reduced to approximately 1 s. Moreover, under sufficiently strong CTR feedback, no transverse magnetization precession is observed following the RF excitation.

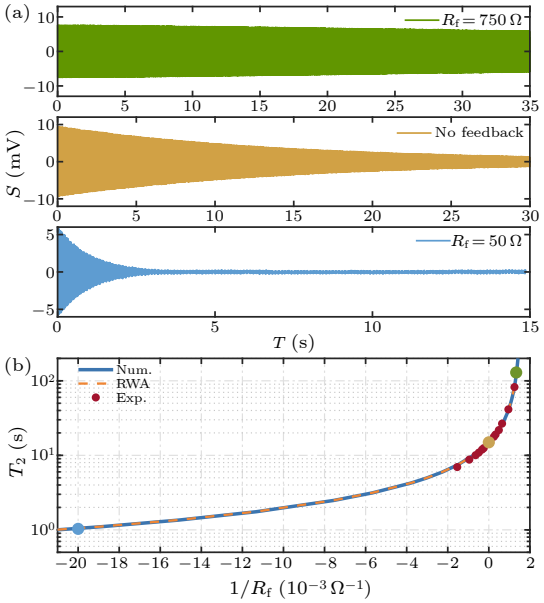

Fig. 3. Feedback-modified ^{3}He nuclear coherence. (a) Typical FID signals at three different feedback strengths. From top to bottom, the signals correspond to the feedback-enhanced, no-feedback, and feedback-suppressed cases. The reduction in T_2 for the suppressed case ($R_f = 50\,\Omega$) is achieved by reversing the polarity of the lock-in amplifier's output signal. (b) Coherence time T_2 as a function of feedback strength, with $G_f \propto 1/R_f$. The solid and dashed lines are the numerical solution and theoretical results, respectively.

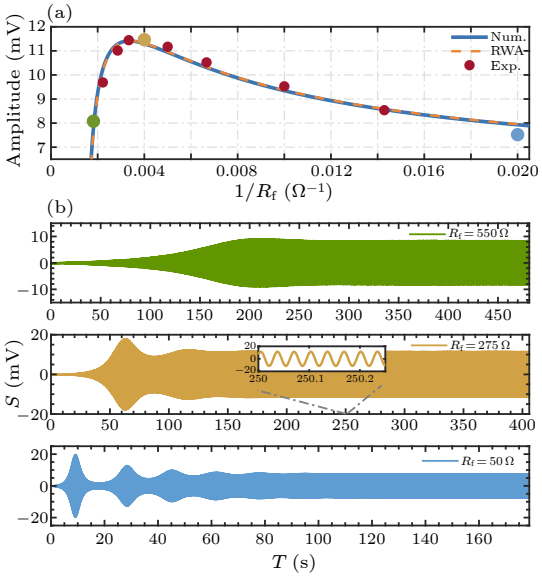

Fig. 4. Feedback-induced maser oscillation of ^{3}He nuclear spins. (a) The steady-state amplitude of the maser as a function of feedback strength with $G_f \propto 1/R_f$. The solid and dashed lines are the numerical solution and theoretical results, respectively. (b) Transient behavior of the maser at three different feedback strengths. The inset plot in the second axis of panel (b) illustrates the oscillation of ^{3}He spin.

In the CTE region, further increasing the feedback strength causes the system to enter the maser oscillation regime. Figure 4(a) presents the steady-state amplitude of the maser as a function of feedback strength. The dashed line corresponds to the prediction from Eq. (6),

while the solid line represents the result from the numerical solution of the feedback-driven Bloch equations. Figure 4(b) displays the maser signals under three different feedback strengths, where the amplitude reaches its maximum at $R_f = 275\,\Omega$. We also observe that, under feedback, maser oscillation can spontaneously build up even in the absence of an initial excitation of the polarized spins. This phenomenon exemplifies self-organization in nonlinear systems.[49] For the feedback-driven Bloch Eq. (1), the nonlinearity primarily arises from spin–spin couplings introduced by the feedback, specifically, through terms proportional to $M_i M_j$. Thus, adjusting the feedback parameters effectively tunes the strength of these couplings. When the coupling strength exceeds a critical threshold, small perturbations in the magnetization are amplified and eventually evolve into a stable, self-organized oscillation.

This nonlinear system exhibits robustness against perturbations, which contributes to long-term stabilization of the oscillation and allows recovery to the steady state after sudden disturbances. We assess the robustness of the spin maser by applying white noise to the x-axis coils and measuring the resulting frequency variation as a function of noise intensity. To quantify the maser's resilience to noise, the following metric is used:[49]

$$\mathcal{R} = \frac{\int \mathcal{S}_0(\omega)\mathcal{S}_\sigma(\omega)\mathrm{d}\omega}{\sqrt{\int \mathcal{S}_0^2(\omega)\mathrm{d}\omega \int \mathcal{S}_\sigma^2(\omega)\mathrm{d}\omega}}, \tag{9}$$

where $\mathcal{S}_0(\omega)$ and $\mathcal{S}_\sigma(\omega)$ are the spectral densities of the oscillation signal with and without noise, respectively, characterizing the similarity between the noise-affected signal and the original one. Figure 5(a) shows the similarity $\mathcal{R}$ between the oscillation signal at different noise levels and that without noise. We can observe that when the noise level increases to $\sim$0.5 V, corresponding to a magnetic field of $\sim$6 mG, the similarity $\mathcal{R}$ decreases to e^{-1}.

We investigated the long-term stability of the maser oscillation by recording the signal for approximately 6000 seconds and dividing it into 0.5 s time slices. By fitting each slice, the oscillation frequency as a function of time is extracted. The Allan deviation of these frequencies is shown in Fig. 5(b). The frequency instability decreases to approximately 7×10^{-5} Hz at an averaging time of 30 seconds but increases thereafter, indicating limited long-term stability of the current maser setup. This degradation may be attributed to the system operating in free-run mode, where fluctuations in parameters such as magnetic field strength and probe laser intensity lead to frequency drift. Nevertheless, the short-term frequency stability of our spin maser reaches approximately 1.7×10^{-4} Hz, which is comparable to that of alkali-noble gas spin masers reported in Refs. [41,50]. The performance of the MEOP-based spin maser is expected to improve substantially if the frequency instability can be reduced by stabilizing the parameters governing its free-run behavior.

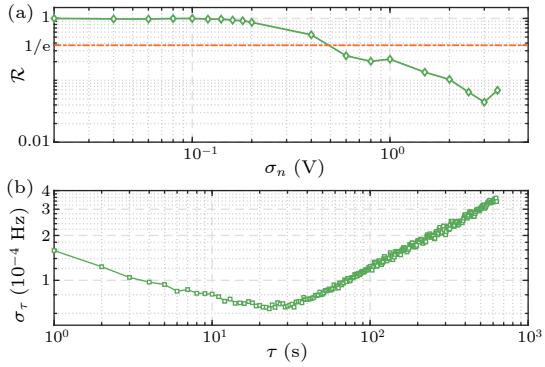

Fig. 5. Robustness and stability measurements of the ^{3}He maser oscillation. (a) Robustness of the maser oscillation frequency under external white noise applied to the system. The similarity $\mathcal{R}$ between noisy and noise-free signals is plotted as a function of noise variance. (b) Allan deviation of the maser oscillation frequency as a function of averaging time, showing frequency stability over durations up to 600 seconds.

5. Conclusion. In summary, we developed a closed-loop polarized ^{3}He system based on MEOP to investigate the influence of feedback on nuclear spin precession under varying feedback strengths and polarities. The spin dynamics under feedback are theoretically analyzed by solving the nonlinear Bloch equations in the steady state within the RWA framework. Experimentally, the feedback is implemented by routing the optical rotation signal—proportional to the nuclear spin precession—back to a pair of RF coils placed close to the ^{3}He cell. The feedback strength is controlled via a variable resistor in the loop. In the decay mode, we observe that the coherence time of the spin precession can be extended by approximately an order of magnitude, potentially enhancing the sensitivity when operating as a nuclear spin-based magnetometer. Conversely, reversing the polarity of the feedback suppresses the spin coherence, which may help reduce measurement dead time in certain applications.

The steady-state amplitude of the maser oscillation is studied as a function of feedback strength, and the optimal condition for sustaining the strongest maser signal is determined. The maser oscillation exhibits robustness against noise. Currently, the frequency stability of the MEOP-based spin maser is about 1.7×10^{-4} Hz over short durations. However, instability appears over longer timescales, likely due to uncontrolled variations in system parameters under free-run conditions. Given the intrinsically low susceptibility of polarized ^{3}He to environmental perturbations—owing to its small atomic radius and closed-shell structure—we anticipate improved long-term stability and enhanced controllability with further refinements to the experimental setup.

Through closed-loop control engineering, our experiment could further unlock the potential of MEOP-polarized ^{3}He for diverse applications. For instance, adapting an artificial pulse feedback scheme or Floquet modulation, a magnetic frequency comb containing multiple oscillation frequencies could be developed, which is useful for accelerating the search for axion dark matter.[51,52] Recently, several experiments have explored the possibility of realizing a continuous-time crystal (CTC) in spin systems using strong feedback, including the Rb-^{129}Xe spin system,[53,54] Rb spin system,[55] and spin system with continuous Larmor frequency distributions.[56] The CTC phase arises from the spontaneous breaking of the system's continuous time-translation symmetry. For example, the feedback-driven Bloch Eq. (1) are invariant under time translation, as none of their terms explicitly depend

on time. However, the maser oscillation predicted by the equation clearly breaks this symmetry, suggesting the possible emergence of a CTC phase. Therefore, the feedback-driven ^{3}He nuclear spin oscillator based on MEOP holds strong potential as a novel platform for studying CTC behavior in spin systems.

Acknowledgments. We gratefully acknowledge helpful discussions with Dr. N. Zhao. This work was supported by the National Natural Science Foundation of China (Grant No. U2230207).

References

[1] Budker D and Jackson Kimball D F 2013 *Optical Magnetometry* (Cambridge University Press)
[2] Farooq M, Chupp T, Grange J, Tewsley-Booth A, Flay D, Kawall D, Sachdeva N, and Winter P 2020 *Phys. Rev. Lett.* **124** 223001
[3] Rabi I I, Zacharias J R, Millman S, and Kusch P 1938 *Phys. Rev.* **53** 318
[4] Schneider A, Sikora B, Dickopf S, Müller M, Oreshkina N S, Rischka A, Valuev I A, Ulmer S, Walz J, Harman Z, Keitel C H, Mooser A, and Blaum K 2022 *Nature* **606** 878
[5] Walker T G and Larsen M S 2016 *Adv. At. Mol. Opt. Phys.* **65** 373
[6] Gao G, Hu J, Tang F, Liu W, Zhang X, Wang B, Deng D, Zhu M, and Zhao N 2024 *Phys. Rev. Appl.* **21** 014042
[7] Graner B, Chen Y, Lindahl E G, and Heckel B R 2016 *Phys. Rev. Lett.* **116** 161601
[8] Sachdeva N, Fan I, Babcock E *et al.* 2019 *Phys. Rev. Lett.* **123** 143003
[9] An FengPeng, Bai Dong, Cai Hanjie *et al.* 2025 *Chin. Phys. Lett.* **42** 11
[10] Tullney K, Allmendinger F, Burghoff M *et al.* 2013 *Phys. Rev. Lett.* **111** 100801
[11] Bulatowicz M, Griffith R, Larsen M *et al.* 2013 *Phys. Rev. Lett.* **111** 102001
[12] Allmendinger F, Heil W, Karpuk S *et al.* 2014 *Phys. Rev. Lett.* **112** 110801
[13] Zhang S B, Ba Z L, Ning D H, Zhai N F, Lu Z T, and Sheng D 2023 *Phys. Rev. Lett.* **130** 201401
[14] Jackson Kimball D F, Budker D, Chupp T E, Geraci A A, Kolkowitz S, Singh J T, and Sushkov A O 2023 *Phys. Rev. A* **108** 010101
[15] Jiang M, Su H, Garcon A, Peng X, and Budker D 2021 *Nat. Phys.* **17** 1402
[16] Sheng D, Li S, Dural N, and Romalis M V 2013 *Phys. Rev. Lett.* **110** 160802
[17] Yi K, Liu Y, Wang B, Xiao W, Sheng D, Peng X, and Guo H 2024 *Phys. Rev. Appl.* **22** 014084
[18] Balabas M V, Karaulanov T, Ledbetter M P, and Budker D 2010 *Phys. Rev. Lett.* **105** 070801
[19] Chen S, Xiang W, Jin X, Xiao W, Peng X, and Guo H 2024 *Phys. Rev. A* **109** 063101
[20] Kominis I K, Kornack T W, Allred J C, and Romalis M V 2003 *Nature* **422** 596
[21] Allred J C, Lyman R N, Kornack T W, and Romalis M V 2002 *Phys. Rev. Lett.* **89** 130801
[22] Jiang M, Huang Y, Guo C, Su H, Wang Y, Peng X, and Budker D 2024 *Proc. Natl. Acad. Sci.* **121** e2315696121
[23] Gemmel C, Heil W, Karpuk S, Lenz K, Ludwig C, Sobolev Y, Tullney K, Burghoff M, Kilian W, Knappe-Grüneberg S, Müller W, Schnabel A, Seifert F, Trahms L, and Bässler S 2010 *Eur. Phys. J. D* **57** 303
[24] Tang Y, Liang C, Wen X, Li W, Xu A N, and Liu Y C 2023 *Phys. Rev. Lett.* **130** 193602
[25] Xu M, Jiang M, Wang Y, Su H, Huang Y, and Peng X 2024 *Phys. Rev. Lett.* **133** 133202
[26] Maiman T H 1960 *Nature* **187** 493
[27] Goldenberg H M, Kleppner D, and Ramsey N F 1960 *Phys. Rev. Lett.* **5** 361
[28] Robinson H G and Myint T 1964 *Appl. Phys. Lett.* **5** 116
[29] Richards M G, Cowan B P, Secca M F, and Machin K 1988 *J. Phys. B: At. Mol. Opt. Phys.* **21** 665
[30] Glenday A G, Cramer C E, Phillips D F, and Walsworth R L 2008 *Phys. Rev. Lett.* **101** 261801
[31] Flowers J L, Petley B W, and Richards M G 1990 *J. Phys. B: At. Mol. Opt. Phys.* **23** 1359
[32] Jiang C, Tong X, Brown D, Lee W, Ambaye H, Craig J, Crow L, Culbertson H, Goyette R, Graves-Brook M, Hagen M, Kadron B, Lauter V, McCollum L, Robertson J, Winn B, and Vandegrift A 2013 *Phys. Procedia* **42** 191
[33] Tang J, Wang B, Huang C, Gao H, Zheng Q, Liu R, Ye F, Qin Z, Wang, T, Salman A, Dong Y, Tian L, Deng C, Li J, Liu L, Qi X, Zhang J, and Tong X 2025 *Chin. Phys. Lett.* **42** 022901
[34] Gentile T R, Nacher P J, Saam B, and Walker T G 2017 *Rev. Mod. Phys.* **89** 045004
[35] Zhang K, Zhao N, and Wang Y H 2020 *Sci. Rep.* **10** 2258
[36] Yoshimi A, Asahi K, Sakai K, Tsuda M, Yogo K, Ogawa H, Suzuki T, and Nagakura M 2002 *Phys. Lett. A* **304** 13
[37] Yoshimi A, Asahi K, Emori S, Tsukui M, and Oshima S 2005 *Hyperfine Interact.* **159** 401
[38] Wang Z, Peng X, Luo H, and Guo H 2017 *J. Magn. Reson.* **278** 134
[39] Sato T, Ichikawa Y, Kojima S, Funayama C, Tanaka S, Inoue T, Uchiyama A, Gladkov A, Takamine A, Sakamoto Y, Ohtomo Y, Hirao C, Chikamori M, Hikota E, Suzuki T, Tsuchiya M, Furukawa T, Yoshimi A, Bidinosti C, Ino T, Ueno H, Matsuo Y, Fukuyama T, Yoshinaga N, Sakemi Y, and Asahi K 2018 *Phys. Lett. A* **382** 588
[40] Inoue T, Furukawa T, Yoshimi A, Nanao T, Chikamori M, Suzuki K, Hayashi H, Miyatake H, Ichikawa Y, Tsuchiya M, Hatakeyama N, Kagami S, Uchida M, Ueno H, Matsuo Y, Fukuyama T, and Asahi K 2016 *Eur. Phys. J. D* **70** 129
[41] Li E, Ma Q, Liu G, Yun P, and Zhang S 2023 *Phys. Rev. Appl.* **20** 014029
[42] Schearer L D, Colegrove F D, and Walters G K 1963 *Rev. Sci. Instrum.* **34** 1363
[43] Cates G D, Schaefer S R, and Happer W 1988 *Phys. Rev. A* **37** 2877
[44] Slichter C P 1990 *Principles of Magnetic Resonance* (Springer Berlin, Heidelberg)
[45] Rubiola E 2008 *Phase Noise and Frequency Stability in Oscillators* (Cambridge University Press)
[46] Wang Y, Wu L, Zhang K, Peng M, Chen S, and Yan H 2024 *Sci. China Phys. Mech. Astron.* **67** 273011
[47] Dupont-Roc J, Leduc M, and Laloë F 1973 *J. Phys.* **34** 961
[48] Kay S M 1993 *Fundamentals of statistical signal processing: estimation theory* (Prentice-Hall, Inc.)
[49] Wang T, Luo Z, Zhang S, and Yu Z 2025 *Commun. Phys.* **8** 41
[50] Chupp T E, Hoare R J, Walsworth R L, and Wu B 1994 *Phys. Rev. Lett.* **72** 2363
[51] Feng M, Wu L, and Liu G 2025 *Phys. Rev. A* **111** 023118
[52] Jiang M, Su H, Wu Z, Peng X, and Budker D 2021 *Sci. Adv.* **7** eabe0719
[53] Wang W, Feng M, Ma Q, Cai Z, Li E, and Liu G 2025 *Commun. Phys.* **8** 191
[54] Huang Y, Wang T, Yin H, Jiang M, Luo Z, and Peng X 2024 arXiv:2411.19561 [quant-ph]
[55] Tang Y, Wang C, Liu B, Peng J, Liang C, Li Y, Zhao X, Lu C, Zhang S, and Liu Y C 2024 arXiv:2407.07697 [quant-ph]
[56] Wang T, Luo Z, Zhang S, and Yu Z 2025 *Phys. Rev. A* **111** 052807